# GFRP Durability appraisal: mechanical testing of panels from the Severn Crossing Visitors' Centre

Pete Gates[a], Tim Ibell[b], Antony Darby[b], Mark Evernden[b]

[a] *Smith Foster Limited, Branksome Park, Poole, Dorset, England*

[b] *Department of Architecture and Civil Engineering, University of Bath, Bath, England*

**ABSTRACT**

Presented are the findings of a durability study undertaken on pultruded GFRP building panels. Sourced, at demolition, from the Second Severn Crossing Visitors' Centre building, these panels offered the rare opportunity to assess the characteristics of naturally aged composite material. Mechanical properties have been determined and compared to the properties of new, equivalent material. The phenomenon of polymer hardening, typified by a reduction in material strain limit over time has also been investigated by further mechanical testing procedures. By contrasting the properties as found for panels taken from each of the four external walls of the building, factors concerning environmental exposure, and factors relating to original fabrication condition have been investigated. Results indicate that regardless of the exposure conditions, in 17 years the mechanical material properties appear not to have significantly diminished, despite aesthetic quality suffering due to lack of maintenance. It has however been shown that UV exposure causes a hardening of the resin component of the composite, resulting in an increase in compressive elastic modulus, but a reduction in the threshold of brittle fracture of the matrix in tension. This final result has not been documented before and is significant in understanding long-term performance of composites.

***Keywords****: Composite structures; Service life; Strength and testing of materials*

# 1 Introduction

The long-term performance of fibre-reinforced polymer (FRP) structures must be assessed if FRP is to win acceptance as a mainstream material for use in the construction industry (Busel 2002). The environmental durability of wholly polymeric structures is often called in to question. In response, accelerated testing is usually undertaken on artificially aged FRP specimens (Boinard et al. 2000; Wang et al. 2010); a lack of genuine naturally-aged material has previously hindered research and validation of material related design life.

Maunsell Structural Plastics produced the eight panels tested in this investigation for application as bridge enclosure panels. Leftover panels, described as 'factory seconds' by the manufacturer, were used to build a site office in 1993, which was later converted into the Visitors' Centre in June 1998, located in an exposed position near the Severn estuary (see Figure 1). Two panels from each of the four principal facades were salvaged for testing upon demolition in May 2009. N, E, S and W (north, east, south and west) denote the elevations from which the panels were taken. Tested in 2010, the results express an account of pultruded GFRP panels naturally aged over 17 years.

A quantitative study assessing the mechanical material properties of panels salvaged from the Severn Crossing Visitors' Centre is intended to address the shortfall in knowledge relating to naturally aged GFRP. The pultruded panels have been tested whole, in flexure, and cut to produce coupons of material for performing a range of mechanical tests. The results produce a profile of the material as a function of both its location within the section (internal flange, web, or external flange), and the aspect of the original location on the Visitors' Centre building. Coupon testing using new, equivalent sample material, has provided a means to assess the mechanical property degradation attributed to exposure in a natural environment. Despite an exhaustive

literature search no 'base case' test data could be recovered to accurately describe the mechanical properties of the aged at the time of manufacture. It was therefore impossible to measure environmental degradation in this way. Resin burn-off has been conducted on the new and aged panel material to aid verification of the extent to which variation observed between these two types is attributed to environmental degradation. The prismatic cellular panels (that are now produced by Strongwell Ltd.) are symmetrical in section (as shown in Figure 2) with an injected foam fill. The fill, which serves to provide a degree of thermal insulation, was applied as an afterthought to improve the environmental performance of the building and is not deemed to enhance structural function. The polymer forming the matrix of the material is polyester unsaturated isophthalic resin. The panel geometric properties, as specified by the manufacturer for both the new and aged panels alike (these specifications have not changed), are shown in Table 1. It has been established, by conducting resin burn-off, that glass fibre content (e-glass fibres) are present in new panels with fibre volume fraction, $V_f$, of approximately 0.36. Full details of fibre volume fractions for the flanges and webs of new and old material are presented in Table 2. The volume fraction of fibres that act as principal longitudinal reinforcement is also shown in Section 2.2.

**Commented [TI1]:** I'd drop this unless you can reference this?

**Commented [PG2]:** This info was received verbally from Strongwell. Shall I ref. a convo., or remove?

**Commented [TI3R2]:** I'd remove the bit about an afterthought.

It should be noted that specific design information from the manufacturer, concerning details of principal, secondary, CSM (chopped strand mat), and surface veil fibre volume fractions was not available. This information is considered confidential by pultrusion manufacturers.

Environmental factors that can cause degradation of the composite include UV irradiation, moisture absorption and thermal fatigue from both diurnal and annual cyclic variations (Karbhari et al. 2003; Compston et al. 2008). South facing panels (see Figure

1) will have experienced the greatest solar irradiation, whilst panels on the north facing façade are expected to have endured the dampest conditions. Panels were missing surface veils (a component present in new panels, responsible for creating a resin rich surface layer during the pultrusion process, to improve aesthetics and durability) on the external face, thus decreasing the expected long-term mechanical performance of this material. This concurs with reports that these panels were earmarked as factory seconds and not used for the primary design purpose in bridge enclosure. A comparative study using internal, external, and web material from each of the façade elevations has been carried out to establish the influence of environmental exposure on the mechanical performance of GFRP pultrusions.

**Commented [TI4]:** Needs a reference.

**Commented [PG5]:** As above; reported by Strongwell. Richard Irvine convo. Shall I cite meeting minutes, or remove? (I'm just unsure as you never really see many references of this sort)

**Commented [TI6R5]:** I'd say 'This concurs with the fact that these panels were..' and forget about a reference, then.

The value of the elastic modulus, $E$, when defined in the field of composites, can be $E_{tensile}$, $E_{compressive}$ or $E_{flexural}$ (Tolf and Clarin, 1984). This is essentially due to the difference between the tensile and compressive moduli of the constituent materials. In this study all forms of the elastic modulus of the aged material have been determined by coupon tests. This allows further exploration of the time dependent properties of the constituent composite parts. Inspecting the results for these relative moduli has prompted further investigation into the occurrence of polymer hardening.

*Figure 1 Left: Location of the four 'panel pairs' from the Visitors' Centre at the Severn crossing estuary. Right: Photo of the southerly elevation*

# 2 Methodology

The methodology used to investigate whole panels is presented first. This is followed by the methodology used for calculation of theoretical strengths and stiffnesses for material at coupon level, followed by coupon testing procedures. The results of the laboratory investigations are then presented in the next section.

## 2.1 Whole panel testing

It was hypothesised that the differing degrees of environmental exposure (in UV irradiation for instance) on the four building facades would yield different reductions in mechanical properties. The properties pursued for comparison were the flexural elastic modulus $E_f$ and flexural shear modulus $G_f$. By establishing values of these properties for each of the panels, the extent of any mechanical deterioration attributed to exposure aspect can be assessed. Table 1 shows sectional geometric properties of the panels, which were tested in flexure to determine $E_f$ and $G_f$.

*Table 1 Panel geometric properties of both new and old panels from manufacturer's design literature (Strongwell, 2010)*

| | | |
|---|---|---|
| Second moment of area, $I$ | | 6620000 mm$^4$ |
| Area, $A$ | | 5740 mm$^2$ |
| Shear Area, $A_s$ | | 1790 mm$^2$ |
| Section depth, $T$ | | 80.3 mm |
| Radius of gyration, $r_y$ | | 33.8 mm |

| | | |
|---|---|---|
| Panel width | | 605 mm |

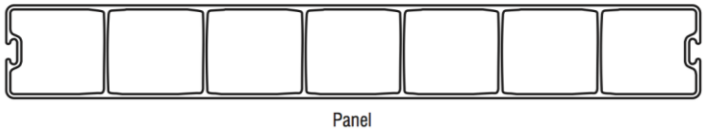


*Figure 2 Strongwell panel cross-section (Strongwell, 2010)*

A test rig for three-point bending was constructed, as shown in Figure 3. Strain gauges were attached to the panel faces at an offset of 150 mm from the central axis of the loading beam. Two gauges on each face (spaced at approximately quarter-width points, with one gauge over a web junction and one between two web locations) were applied to measure an average compressive and tensile strain across the width of the flanges. Three transducers were set up across the panel width to measure the average mid span deflection. Readings from all instrumentation were recorded every second. Three bearing plates, all 150 mm wide, spanned the entire panel width; one under a pinned loading plate beneath the central loading ram, and one at each end, consisting of a pin and roller support plate, forming the simply supported ends of the set-up, as shown in Figure 3.

To determine the flexural elastic modulus and shear modulus, $E_f$ and $G_f$, a graphical method based on the Timoshenko Beam Theory for thin walled sections (Bank, 1989) has been adopted. Each panel was tested over three different spans consecutively before being turned over to repeat testing. Timoshenko's Beam Equation can be re-arranged to produce the following relationship:



(1)

$$\frac{4Aw}{Pl} = \frac{1}{12E_{flex}}\left(\frac{l}{r}\right)^2 + \frac{1}{G_{flex}}$$

*Equation 3.1*

where $l$ is the span length, $P$ is the load applied, $w$ is the mid span deflection, and the other variables are as per Table 1. Each load deflection result can be plotted on a graph of the type shown in Figure 4.

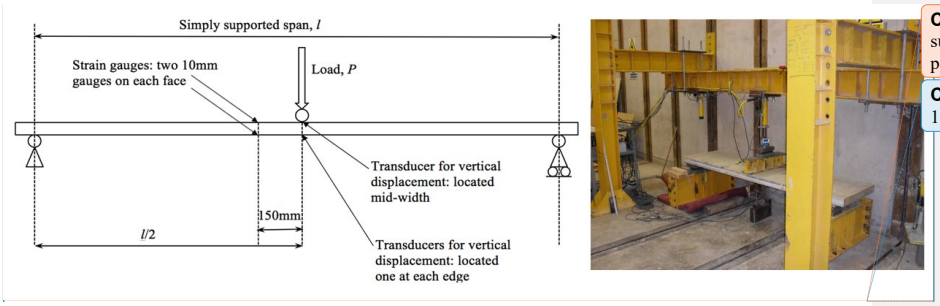


*Figure 3 Three-point loading test rig set-up*

Commented [PG7]: I have a set of images at higher res for submission. Will check the text, and upload as vector if permitted.

Commented [TI8]: Make sure that all font sizes are at least 10 in figures, tables and captions.

A three-point bending set up is used because it means a great proportion of the resulting displacement is attributed to shear deflection, and as a consequence the accuracy of the value obtained for shear modulus is improved.

The flexural elastic modulus and flexural shear modulus can then be inferred graphically from the gradient and vertical axis intercept respectively. Panels were testing in both orientations (with each face uppermost) to investigate whether the

resulting mechanical properties of the weathered external face influenced a different mechanical performance, dependent on whether that face was in tension of compression.

Panel length dictated the maximum span for three-point testing to be 2.1 m with subsequent span reductions of 80% and 60%. Testing over these spans permitted formation of plots such as that shown in Figure 4, producing three well spread data points that were used to define the position of a line of best fit. The gradient of this line is equal in value to $1/12E_f$ and the y-axis intercept is equal in value to $1/G_f$. Hence, the values of the flexural elastic modulus and flexural shear modulus can be obtained.

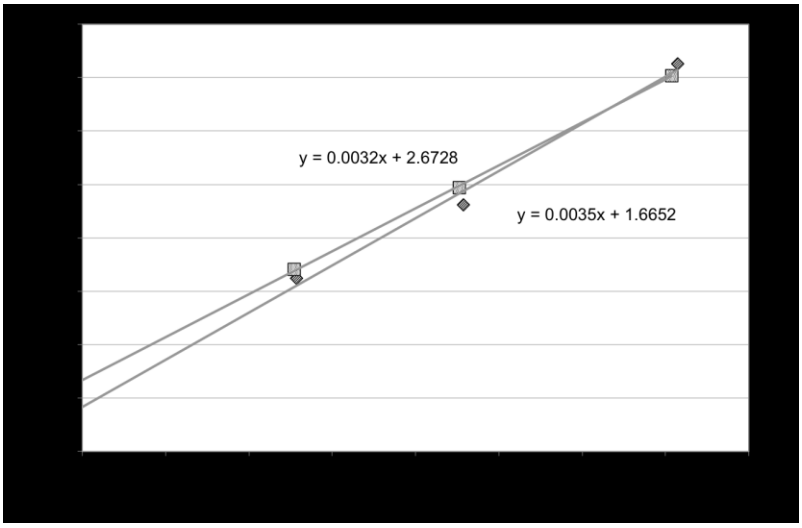


*Figure 4 Graphical plot of Equation 1 for an East-facing panel. (Squares represent tests with external face up and diamonds represent tests with internal face up.)*

Following the flexural tests detailed above the panels were loaded to failure, using the longest of the three simply supported spans described previously. Panel pairs from each façade orientation were tested in alternate orientations in the test rig (one with the

weathered external face uppermost and one with this face down-facing in tension, to observe the anticipated lower failure load when this face was in tension).

### 2.2 Determining relative theoretical mechanical properties by resin burn-off

Stiffness and strength of pultruded GFRP is closely related to fibre content. By establishing the fibre content of material from different parts of the panel cross section, and finding out if there is any inter panel variation in the material fibre content, the relative performance of the coupons can be predicted in mechanical tests. Specimens for testing were cut from webs and flanges of each of the panels. The specimens were 25mm square in size, and sourced at location away from the flange-web junctions of the cellular panels.

For both the aged and new material, resin burn-off to establish fibre weight fraction has been conducted according to ASTM code D 2584-02. After weighing to find the initial mass of each of the 25 mm square samples, each sample was ignited by heating in a crucible over a Bunsen flame and left until the volatiles had cleared (once the smoke had stopped) and only the fibres, ash and carbon remained. Each sample, in its own crucible, was then placed in a muffle furnace at 565$^{o}$C until all the carbonaceous material had disappeared (see Figure 5). Six hours was sufficient for this. Re-weighing of the remaining fibres yielded the fibre weight fraction, and using values for the fibre and matrix density, (2570 and 1200 kg/m$^3$ respectively (Bank, 2006)), the volume fractions could then be determined.

*Figure 5 The sample was ignited using a Bunsen Burner (left, and then later placed into a muffle furnace (right)*

Principal fibres, chopped strand mat, and surface veils (present on only new composolite panel material) were separated to enable more accurate calculation of volume fractions and subsequent theoretical mechanical properties, as others have recommended (Ye et al., 1995). Fillers have not been removed, however, as this entails procedures of chemical washing and then drying, such that the chopped strand matt (CSM) fibre fractions are known to be overestimates.

Three samples were subjected to resin burn-off for each of the locations specified in the first column of Table 2. 'Int' denotes internal flange material, which relates to the orientation of panel and material from the interior facing surface. In the same vein 'Ext' refers to flange material that was taken from the exterior face of the panel.

Not all façade aspects are represented in this testing, but the aged panels were all manufactured to the same specification. Whilst the degree of variation observed between material from facades of different aspect and panel location (internal or

external) is revealed, it is the average fibre content values for flange and web material, of the new and aged panels, that was required to establish the desired theoretical properties of relative mechanical performance.

The volume fractions presented in Table 2 are mean values derived from the results of three coupon specimens. The results from coupons taken from the north facing façade web elements (highlighted in grey in Table 2) are not included in the averages for aged webs owing to the large standard deviation in those results. The distribution of principal fibres in many of the web elements tested was not uniform, but as illustrated by Figure 6, it can be seen that the principal fibres (seen as darker fibres in the image) in the web are lying in bunches. Samples for testing taken from these webs capture various amounts of these fibres, rendering a reduced confidence in the average value yielded. This was especially true for web samples taken from panels originally on the north facing façade.

*Table 2 Fibre volume fractions for the flanges and webs of new and old material*

| Coupon location | Total fibre volume fraction, $V_f$ | Principal fibre volume fraction, $V_{pf}$ | Standard deviation |
|---|---|---|---|
| Int flange E | 0.40 | 0.24 | 0.014 |
| Int flange S | 0.38 | 0.26 | 0.024 |
| Int flange W | 0.40 | 0.24 | 0.046 |
| Ext flange E | 0.37 | 0.21 | 0.012 |
| Ext flange S | 0.40 | 0.26 | 0.015 |
| Ext flange W | 0.36 | 0.22 | 0.008 |
| Ext flange N | 0.38 | 0.24 | 0.003 |
| | **Aged flange average** | **0.24** | |
| Web E | 0.39 | 0.18 | 0.003 |
| Web S | 0.29 | 0.09 | 0.016 |
| Web N | 0.38 | 0.16 | 0.087 |
| | **Aged web average** | **0.14** | |
| **Flange new** | 0.36 | 0.25 | 0.041 |
| **Web new** | 0.34 | 0.24 | 0.026 |

New composolite panels appear to be fabricated with a similar proportion of principal fibres in the flange and the web elements; see bottom two rows of Table 2. The aged panels, although possessing a similar fibre content in the flanges, exhibited reduced fibre fraction in the webs. Thus, the stiffness and strength predicted for the aged webs are approximately 67% that of the aged flanges, which is indicative of how they were manufactured. It should be noted that a reduced amount of principal fibres were found to exist in the web elements from the southern façade panel tested, and as with other webs examined the distribution was not uniform, but as illustrated in Figure 6. This represents a high degree of inter-panel variation in the manufacturing of the webs in the aged panels, as well as intra-panel variation.

**Commented [PG9]:** See last two rows of table. Direction added to text.

**Commented [TI10R9]:** Perfect.

**Commented [TI11]:** Needs a reference and/or the volume fractions achieved on average today.

The resin burn-off results verify that variation in mechanical performance observed between new and aged flanges can be observed chiefly as a consequence of ageing rather than differing fibre contents. One large manufacturing difference is evident. In Figure 7 the additional layer (surface veil) present in the new material can be distinguished easily by eye, from the CSM and the principal fibres, once removed from the furnace. The surface veil was known to be present in the original composolite panel design to create a resin rich surface layer to enhance environmental durability. It was not found in the aged panels, however, that are understood to be factory seconds, and hence not used for the intended application of bridge enclosure.

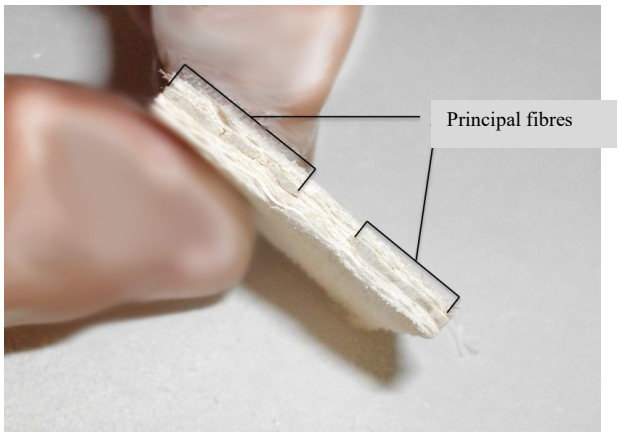


*Figure 6 Principal fibres visible within the aged web coupon cross-section, after removal from furnace. Principal fibres are in the direction perpendicular to the page.*

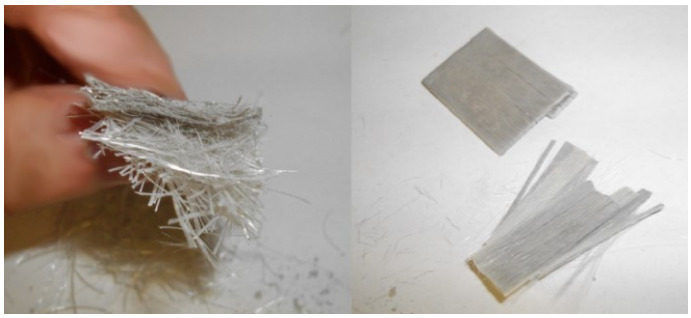

*Figure 7 Fibres from new material. Left: Surface veil over CSM Right: Principal fibres*

### 2.3 Tensile testing of coupons

To compare the mechanical properties of material from different panel locations, and compare new and old material the axial tensile strength and modulus were two properties determined by fabricating and testing coupons in tension. These properties are influenced mainly by the fibre component.

Three coupons representing each of the internal and external flange material, and web material, for each façade aspect, were cut from near the panel ends, which had not experienced significant bending stresses from the previous whole panel testing (less than 20 MPa; ~ 10% of the ultimate tensile strength from Strongwell (2010) literature.) The average thickness of the flange coupons was 3.15 mm, and of the web coupons 2.66 mm. The precise cross sectional geometry of each coupon was measured using Vernier calipers. Coupons were sized at 25 mm wide × 250 mm long according to BS EN ISO 527 (BSI 2009), with the pultruded fibres (0 degree fibres) aligned along the coupon length. Aluminium tabs of 1.5 mm thickness and 50 mm length were bonded to the coupon ends (in the area in contact with the test rig jaws) using epoxy resin. A single 10 mm strain gauge was attached centrally on each face of the coupon, orientated in the direction of the applied load. Testing was conducted under displacement control at 1 mm/min, in line with both manufacturer testing and the code-based approach adopted. Coupons extracted from new, equivalent panels, manufactured by Strongwell, were also tested for comparison.

### 2.4 Compressive testing of coupons

To further compare the mechanical properties of the various categories of material (as described above) the axial compressive modulus was determined. This property is influenced more by the resin component than tensile properties are, and so permits the opportunity to assess environmental degradation of the resin.

A test rig used to clamp the ends of the coupons was fabricated to prevent rotation whilst loading the sample through its ends, as shown in Figure 8. For testing in compression, the overall coupon length was 165 mm (again, aligned such that the

pultruded fibres were aligned along the coupon length) and 10 mm width, with 70 mm of each end clamped in the rig, and 25 mm left clear. Strain gauges were attached using cyanoacrylate cement, a single component room-temperature curing adhesive, one to each face of the coupon in this free region. Testing was again conducted under 1 mm/min displacement control. Results for ultimate compressive stress are not included, only compressive elastic modulus, because buckling prevented the determination of accurate material compressive strength. Shorter specimens would have enabled ultimate compressive stress to be established, however they would require smaller gauges that would not be accurate in determining the elastic modulus. Further tests would be required to achieve this.

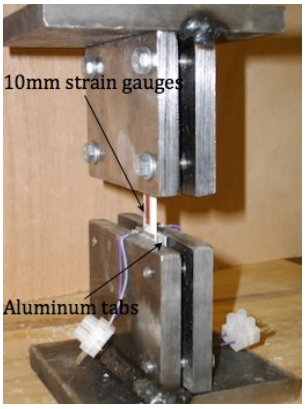


*Figure 8 Coupon setup for compression test rig*

### 2.5 Shear testing of coupons

Shear testing is a resin dominated mechanical test of the composite material. The Iosipescu Shear Test (Vishay 2008) procedure was adopted to perform testing. A custom rig was designed to accommodate suitable coupon sizes and to apply a shear force in line with the Iosipescu methodology, as shown in Figure 9. Principal (0 degree) fibres were once again aligned parallel with the longitudinal specimen direction

(perpendicular to the load direction). Two steel plates provided out of plane stability to the test specimen. The specimens were 20 mm wide × 100 mm long. Top and bottom steel loading bars, together with a pin arrangement, enabled loading to be applied to produce maximum shear and zero moment at the centre point of the test coupon. An observation window cut-out allowed strain gauges to be located effectively. The pins were located within long slotted holes to guide them, avoiding the need to notch the sample at the pin locations, which could otherwise have caused unwanted stress concentrations due to the notch inhibiting lateral movement of the pin across the surface under flexure. The specimen was loaded by means of a mass hanger and weights, with the load applied through the top pin of the rig. Loading was limited to 80 kg by the strength of the loading system, and it was found that this could be applied accurately without damaging the rig. The geometry of the loading arrangement results in a shear force, in the measured region, of 80% of the applied load, as shown by Equation 2 and illustrated in Figure 9.

$$\text{Shear} = b_s - a_s = 0.9F - 0.1F = 0.8F \tag{2}$$

Where $a_s$ and $b_s$ are locally applied point loads inducing shear in the specimen.

Readings from two perpendicular 45° strain gauges were recorded and the shear modulus $G_{xy}$ calculated according to Equation 3. This equation is true for any inclination of shear plane in the specimen (as a result of variation in the specimen depth), providing the gauges are centred at mid depth at the point of contraflexure of the specimen.

$$G_{xy} = \tau_{xy}/(\varepsilon_1 - \varepsilon_2) \tag{3}$$

Where $\varepsilon_1$ and $\varepsilon_2$ are strains from the two perpendicular gauges inclined at 45° to the horizontal, and $\tau_{xy}$ is the shear stress at mid depth of the section found from the section dimensions, and the shear force as per Figure 9. Equation 4 is taken from a technical note for use of strain rosettes in performing Iosipescu tests (Vishay, 2008), and accounts for the influence of the vertical compressive strain when using gauges inclined at 45° to determine shear strain, $\gamma_{xy}$, where α is the inclination angle of the gauge, thus explaining why $\gamma_{xy}$ is represented as ($\varepsilon_1$ - $\varepsilon_2$) in Equation 3.

$$\gamma_{xy} = (\varepsilon_1 - \varepsilon_1)/\sin 2\alpha \tag{4}$$

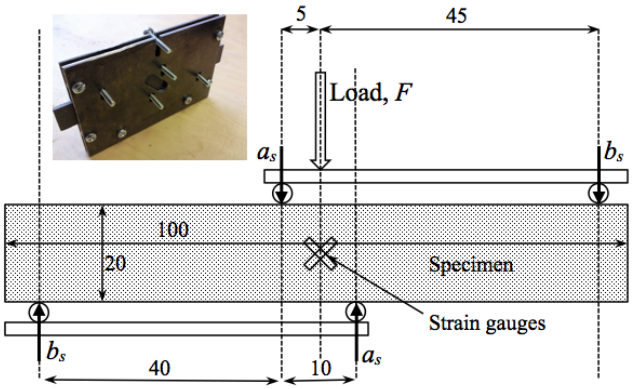

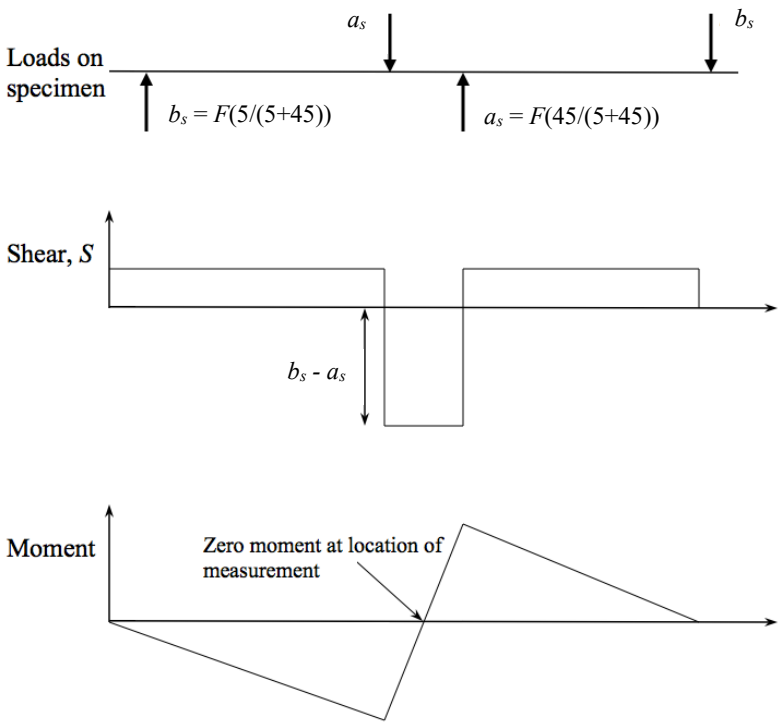


*Figure 9 Iosipescu shear rig set-up (all dimensions in mm). Schematic showing how loads on specimen are achieved and shear is derived at zero moment location*

# 3 Results

## 3.1 Design values for new composolite panel properties

Design values for the Composolite panels, as manufactured today, are stated in the Strongwell design literature (Strongwell, 2009). Table 3 shows values related to stiffness and strength. Also obtained from the manufacturer's literature are the results of three-point bending tests performed on complete panels, equivalent to the testing undertaken on the aged panels. By performing the graphical method describing Timoshenko Beam Theory on these results, further values (also included in Table 3)

have been established for comparison.

*Table 3 GFRP material properties (Strongwell, 2009)*

| Strongwell design literature (min value) | | |
|---|---|---|
| Tensile elastic modulus, $E$ | | 17.1 GPa |
| Ultimate tensile strength | | 214 MPa |
| $E_{flex}$ and $G_{flex}$ inferred by graphical method from Strongwell's in-house load-deflection test results | | |
| Flexural elastic modulus, $E_{flex}$ | | 25.3 GPa |
| Flexural shear modulus, $G_{flex}$ | | 0.95 GPa |

### 3.2 Whole panel testing: flexural elastic modulus

Figure 10 and Figure 11 provide a summary of results concerned with flexural stiffness. Each bar represents the value for a single panel. A single panel from each façade elevation has been tested over three spans in three point bending, with the exposed face in tension, and then again with the exposed face in compression, according to the procedure described in Subsection 2.1.

Figure 10 shows panels that have experienced direct UV irradiation (on the east, south and west facing building elevations,) exhibit a lower stiffness when tested in bending with the exposed external face in tension. The north facing panels do not show this behaviour. This suggests that degradation attributed to UV exposure, or cyclic wetting and drying, is of greater detriment to material stiffness when compared to damp conditions alone. It also suggests that in tension the matrix is compromised, however in compression it is not.

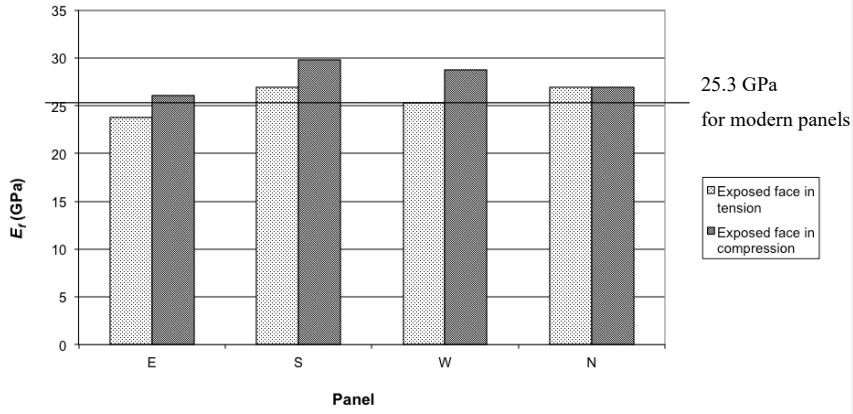


*Figure 10 Flexural elastic modulus for each of the building panels, and the manufacturer's testing derived value of 25.3 GPa*

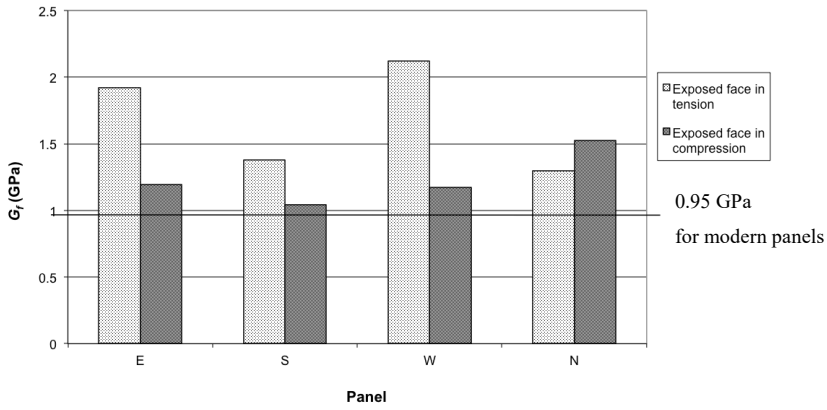


*Figure 11 Flexural shear modulus G for each panel, as per original orientation on building, and nature of test and the manufacturer's testing derived value of 0.95 GPa*

Examining the results of Figure 11, the calculated flexural shear modulus appears to be sensitive to the nature of testing of the panel (inverted or not). However, it has

previously been documented (Tolf and Clarin, 1984) that the shear modulus values derived using the graphical method employed are sensitive to small changes in the fit of the regression line. Considered mathematically, the adopted Timoshenko equation for beam bending produces a solution for flexural shear modulus that is highly sensitive to small changes in the input variables, due to the small contribution of shear deformation to the total deflection. The average shear modulus measured does appear to meet that of the manufacturer's value for modern panels. See Figure 11.

### 3.3 Coupon testing: tensile modulus

Figure 12 shows the results of coupons taken from the panels and tested in tension. The web material of the aged panels appears to have a lower tensile modulus compared to flanges, though this difference is not evident in the new material. This is as predicted by resin burn off and hand calculation. The lowest value of tensile elastic modulus established during testing was 15 GPa (for the south facing panel web coupons). This correlates well to the established reduction in fibre content of these elements as illustrated in Table 2. Coupons of internal material out-perform those of external material from both south and west facing panels, subjected to the prevailing estuary wind. Coupons from north and east facing panels do not exhibit this trend. A large variance across tests is observed, particularly for the webs (as already discussed) and external material, prompting further investigation. Each result represents an average from three coupon tests.

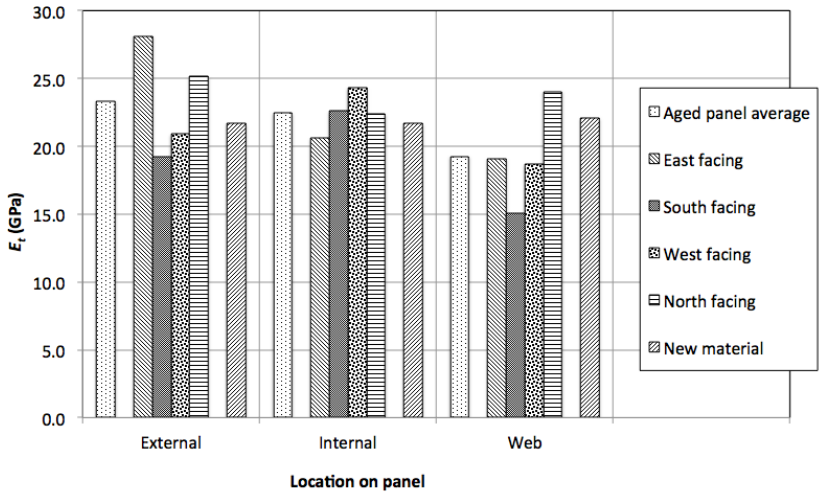


*Figure 12 Tensile elastic modulus as a function of coupon origin*

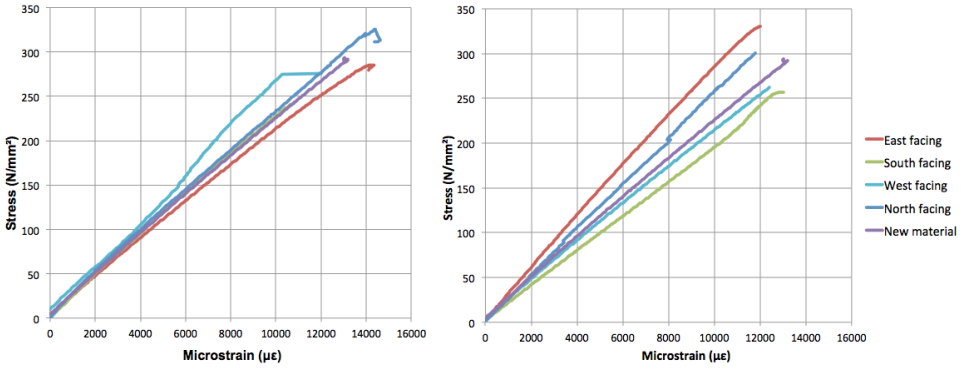


*Figure 13 Stress-strain plots, for internal (left) and external (right) panel material*

Figure 13 shows a high degree of linearity to failure in the stress-strain response of the pultruded GFRP to axial tensile load. It should be noted that not all of the plots presented in this figure represent the material to failure due to strain gauges going off-scale or breaking from the specimen before this, and tensile elastic modulus was calculated using a strain of 2000 με.

### 3.4 Coupon testing: tensile strength

Figure 14 portrays the strength of material from different panel origins. Coupons of external flange material exhibited a lower strength when compared to internal ones, indicative of environmental degradation. Material that was exposed on the south facing building façade shows the biggest reduction in strength. This material has been subjected to the most UV irradiation. Each result represents an average from three coupon tests.

As also found in the tests measuring tensile elastic modulus, webs from the south facing panels tested gave a low result, by chance equal to the lower-bound manufacturer's design value (214 MPa), which again, correlates well with the reduced fibre content of these elements established by resin burn-off.

Tensile strength and modulus exhibit similar trends, indicating that perhaps fibre volume is responsible for the variation, rather than degradation. Table 2 shows that this is probably not the case, and that environmental degradation is indeed responsible. The south facing external flange material that was subjected to rein burn-off possessed the highest fibre content. The crucial finding here is that the average aged-panel tensile capacity (293 MPa) is significantly lower than the new-panel tensile capacity (321 MPa).

**Commented [TI12]:** From Figure 14, the right hand bar seems to be much higher than 321 MPa? 390-ish MPa?

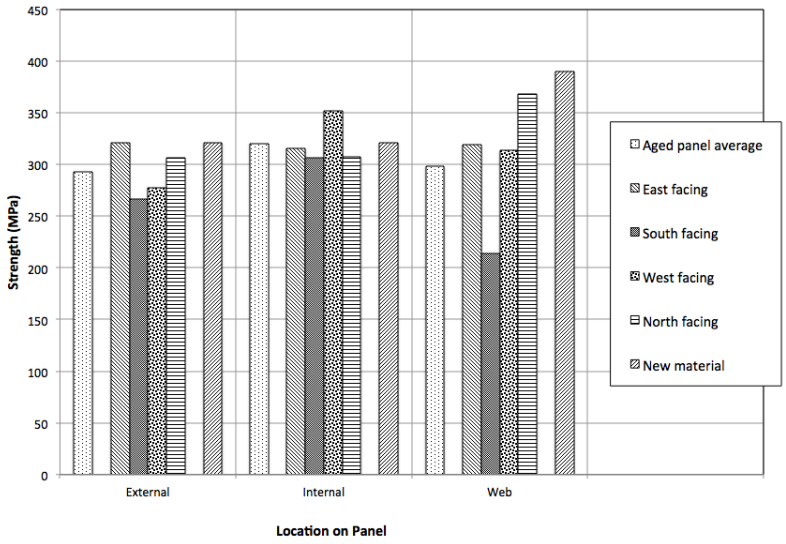


*Figure 14 Maximum tensile strength of coupons*

### 3.5 Coupon testing: compressive modulus, $E_c$

The compression modulus data presented in Figure 15 is the minimum value determined from the two coupons tested to establish each data point. A high level of variation was shown between the two coupons tested for south facing panel webs (41.9 GPa and 15.5 GPa, resulting in a standard deviation of 18.7 GPa). This supports the existence of a non-uniform distribution of principal fibres in the web material of the south facing panels (the next largest standard deviation of only 3.7 GPa was for web coupons from the east facing panels.) The fabrication variability in this web material, attributed to the reduced quality control (they were 'seconds') is seen to impinge on the mechanical properties. The limited width of coupons extracted (10 mm for compressive testing), and the distribution of fibres in the webs, as shown in Figure 6, is understood to permit large variations in the amount of fibre 'captured' in the prepared test specimen.

Thus the degree of variability exhibited in results for web specimens is amplified.

The overall average compressive elastic modulus of 26.8 GPa was 17.5% higher than the tensile modulus determined in Subsection 3.3. It is more usual that compressive modulus is lower than tensile modulus for FRP materials (Bank, 2006), so this suggests that, in this case, the resin is playing an important part in the behaviour. The resin component, which would not contribute much to the measured modulus in the new material, could be contributing to compressive stiffness to a greater extent than tensile stiffness, owing to physical change with age. A hypothesis explaining this outcome is presented and tested in Section 4.

No new material was available by the stage of compression testing for comparison. A standard deviation of 2.1 GPa was found for average results relating to panels on different facades, in both tensile and compressive testing for elastic modulus. In tension, however, the panel webs displayed a lower average stiffness compared to the panel flanges, which is not evident in results for compressive testing. This suggests that the resin is of greater influence on the compressive modulus measured than the tensile modulus. The compressive strength was not measured due to test limitations resulting in premature buckling of the specimens.

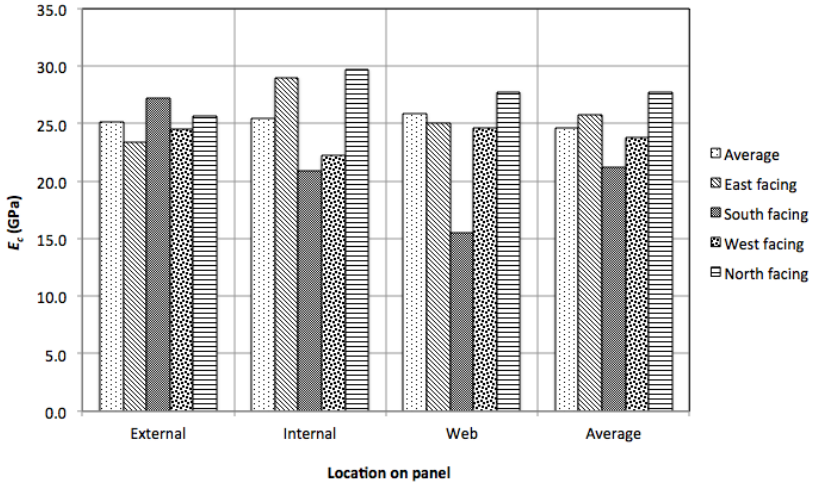


*Figure 15 Compressive modulus, $E_c$ as a function of coupon origin*

### 3.6 Coupon testing: shear modulus

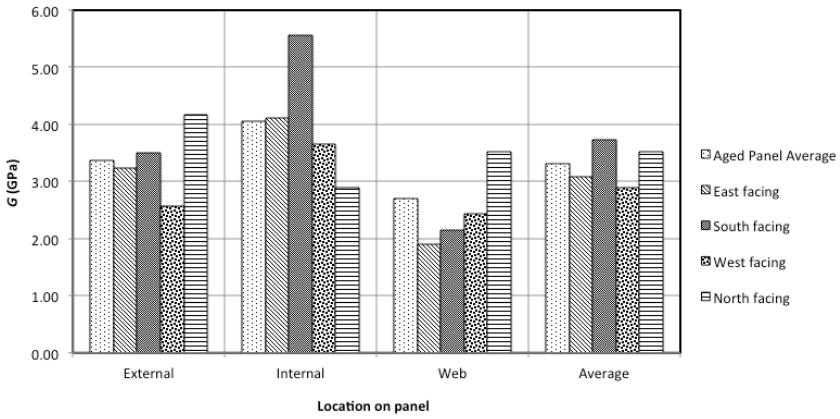


*Figure 16 Shear modulus as a function of coupon origin*

Figure 16 shows the results of the shear modulus coupon tests. It can be seen that the west facing panels exhibit the lowest average shear modulus. The lack of stiffness of webs in this panel is not likely to be attributed to deterioration with age, as the exterior material has maintained good integrity. Internal coupons were observed to be stiffer than external coupons by 17%, although the averages displayed are affected by the result for the internal coupons from south facing panels.

### 3.7 Flexural strength of whole panels

A model was derived, from first principles, for the bending stiffness of cellular panels (of the type investigated above in section 3.2). See figure 17. Previous studies have reported that the axial compressive stiffness is typically 80% that of the tensile stiffness (Bank, 2006), and the model takes into account this ratio of differing compressive and tensile axial elastic modulus of the fibres in the GFRP. It has been demonstrated in Section 3.2 that the aged resin influences the relative compressive and tensile elastic moduli to an extent where the fibre behaviour does not yield a similar effect on composite stiffness. This section details work undertaken with the intention of comparing failure stresses for each of the panels, and also comparing the theoretical flexural response of panels according to a compressive/tensile modulus ratio from literature, with a measured experimental response. This second objective was not possible, for reasons explained below. It has been shown that the model developed to describe the stress and strain in the composite section is useful in comparing the performance of panels from each façade orientation, to observe whether environmental exposure has influenced ultimate collapse load.

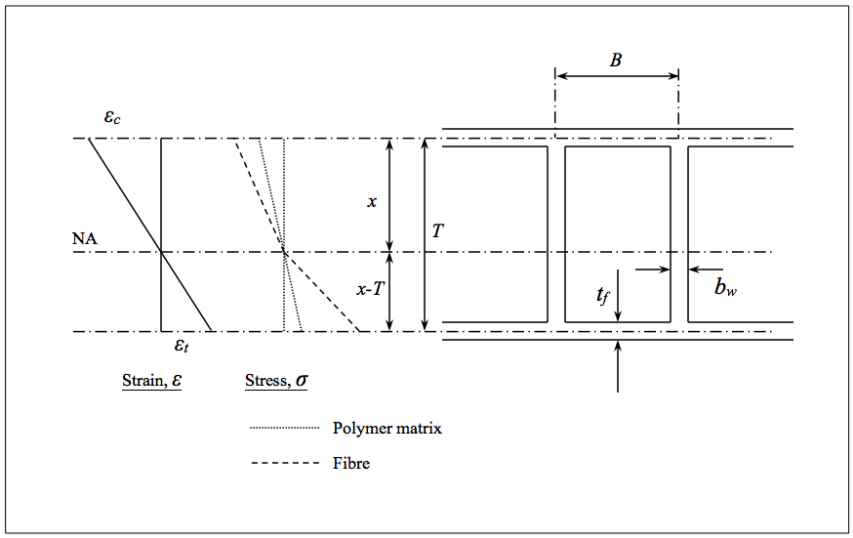


*Figure 17 Stress block for FRP thin walled section*

$$x^2\left[E_{fc}\left(\frac{b_w}{2B}\right)V_f + E_m\left(\frac{b_w}{2B}\right)(1-V_f)\right] - (T-x)^2\left[E_{ft}\left(\frac{b_w}{2B}\right)V_f + E_m\left(\frac{b_w}{2B}\right)(1-V_f)\right]$$
$$+ (T-x)\left[E_{ft}t_fV_f + E_mt_f(1-V_f)\right] - x\left[E_{fc}t_fV_f + E_mt_f(1-V_f)\right] = 0 \quad (5)$$

Table 4 shows values relating to the properties of the Composolite building panels that are necessary to determine the neutral axis depth and moment of resistance per unit surface strain according to Equation 5 (from which the neutral axis x may be found) and the stress distribution in Figure 17. The resulting value of 9,800 kNmm/mm was used together with the 3-point test span, and the predicted failure load found experimentally for each panel, to provide an expected strain at failure on the compressive upper panel face. Note that the figure 9,800 kNmm/mm is a moment per unit width, per unit strain on the surface in compression. Table 5 shows how this was used to determine failure strain and stress: the values in the column for compressive

strain are found from the moment per unit width of panel divided by the value 9,800 kNmm/mm.

The model in Figure 17 allows comparison of theoretical values for surface strain with measured values in the laboratory. Table 6 shows this expected strain at failure, alongside average measured strain at failure from the two gauges present on the upper surface of each panel.

*Table 4 Composolite panel properties. Neutral axis depth and resistive moment per unit surface strain, as calculated theoretically.*

| $T$ (mm) | $B$ (mm) | $t_f$ (mm) | $b_w$ (mm) | $V_f$ | $E_m$ (GPa) | $E_{ft}$ (GPa) | $E_{fc}/E_{ft}$ | $E_{fc}$ (GPa) | $x$ (mm) | M/ε/unit width (kNmm/mm) |
|---|---|---|---|---|---|---|---|---|---|---|
| 77.1 | 85 | 3.15 | 2.66 | 0.67 | 3.6 | 75 | 0.8 | 60 | 44.0 | 9.80E+03 |

*Table 5 Failure strain and stress, derived from load, test span and theoretical distribution of stress*

| Panel façade | Nature/orientation | Failure load (kN) | Length of span (mm) | Moment per unit width Nmm/mm | Compressive strain (as per table 3.4) (microstrain) | Comp. fibre stress (as per $E_{fc}$ = 60GPa) (MPa) |
|---|---|---|---|---|---|---|
| E | Int. in comp. | 36.8 | 2010 | 30571 | 3120 | 187 |
| | Ext. in comp. | 52.1 | 2010 | 43282 | 4417 | 265 |
| S | Int. in comp. | 49.5 | 2090 | 42815 | 4369 | 262 |
| | Ext. in comp. | 40.5 | 2100 | 35200 | 3592 | 216 |
| W | Int. in comp. | 34.5 | 2090 | 29810 | 3042 | 183 |
| | Ext. in comp. | 43.0 | 2110 | 37499 | 3826 | 230 |
| N | Int. in comp. | 37.1 | 2560 | 39259 | 4006 | 240 |
| | Ext. in comp. | 32.4 | 2550 | 34182 | 3488 | 209 |
| | | | | | average: | 224 |

*Table 6 Compressive strain at failure for each panel and orientation, based on failure load and theoretical model, alongside average of two strain gauge measurements ('*' indicates that a gauge peeled from the specimen or went off-scale prior to failure, so that the value represents the single remaining gauge)*

| Panel | Strain at failure (με) | | | |
|---|---|---|---|---|
| | Internal face up | | External face up | |
| | Predicted from model | Measured | Predicted from model | Measured |
| E | 3120 | 2510* | 4420 | 4010* |
| S | 4370 | 3840* | 3590 | 3120* |
| W | 3040 | 2870 | 3830 | 3540* |
| N | 4010 | - | 3490 | 3100 |

It can be seen from Table 6 that the measured strains are below those predicted from the theoretical model. This implies that the neutral axis position was closer to the compressive face than expected at (or just before) failure.

To quantitatively assess the extent to which the neutral axis had migrated from its expected position more accurate strain gauge readings would be required. It is concluded that the work above cannot verify this. However the findings do seem to align with previous results in this paper indicating that the GFRP polymer matrix was susceptible to brittle fracture in tension (causing the neutral axis to be closer to the compressive face than expected).

The results obtained for failure strain using the theoretical model are of much greater use to compare stress in the panels at failure; relying not on strain gauges, but on measured load, and panel and testing geometries. Figure 18 shows the data inferred by the failure load and the model.

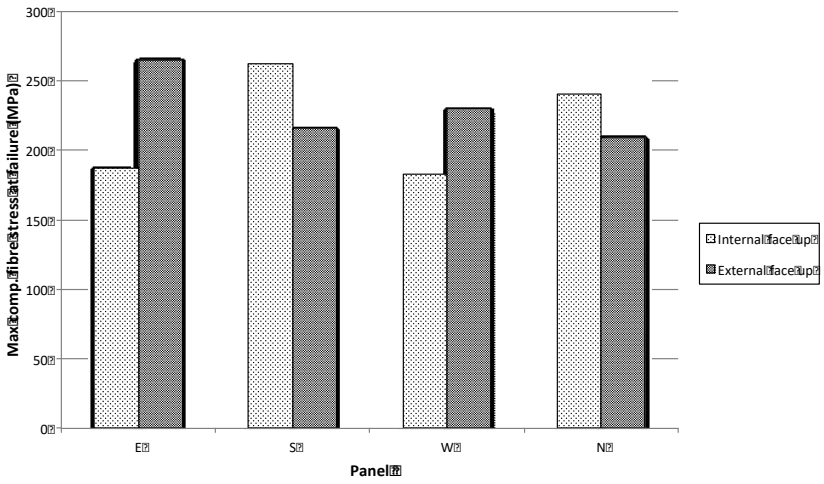


*Figure 18 Max compressive fibre stress at failure of whole panel in three-point bending*

The strength of the panels does not appear to be affected by the original aspect or orientation of testing as seen with the stiffness of whole panels. However, it should be noted that failure of the panels was by flange buckling with accompanying tearing of the flange web junction. This type of failure is very unstable and sensitive to a large number of variables. The large scatter in results attributed to this means that a larger number of panels would need to be tested to destruction to make the same kind of conclusions regarding the influence of environmental exposure as could be made regarding the stiffness of the whole panels.

# 4 Assessment of polymer hardening

## 4.1 Introduction

Brittle hardening of the polymer resin appears from the results in this paper to have significance in relation to the whole life performance of GFRP. It is not a phenomenon that has yet been documented as being significant in existing literature.

Upon inspection of the results from the coupon testing, the measured *compressive* elastic modulus (26.6 GPa mean value) was found to be higher than the *tensile* modulus found for the material (22.1 GPa mean value). An entirely opposite relationship had been expected, since micro-buckling of fibres typically reduces elastic modulus in compression; a value in compression of approximately 80% that of the tensile modulus is more typical (Bank, 2006). It was hypothesised that brittle hardening of resin over time may be responsible. The external material from the south facing panels, which had experienced a higher degree of UV irradiation, exhibited the highest modulus. Hardening of the resin with age, and with UV exposure, could explain a higher modulus when working in compression. Such hardening could result in a reduced stiffness in tension due to early onset of brittle facture in the resin, whereas in compression no such fracture occurs. To investigate this hypothesis, further experimental work was undertaken.

## 4.2 Procedure for assessment of polymer hardening

Three coupons of aged GFRP external flange material, from south facing panels, and five coupons of new GFRP Composolite panel flange material, were subjected to two identical flexural tests (see Figure 19), each with intervening tensile loading. The tensile

loading was undertaken in accordance with the method described previously in Section 2.3, but with samples 330 mm in overall length. The tensile strain to which each coupon was subjected was varied according to values indicated in Table 7 and Table 8. The influence of the direct axial tensile strain could be observed by changes in the response of subsequent flexural tests, i.e. if resin plasticity was preserved there should be no fracture of the resin and the initial and final flexural tests should correspond to identical flexural moduli. If UV degradation of the resin over the material lifetime had caused a brittle hardening, and the strain limit of tensile fracture of the resin was exceeded then a variation between the two flexural responses (pre and post tensile test) would be evident.

These flexural tests were conducted over a 200 mm span such that the strain in all material remained below 4000 με, which corresponds to a stress of 87 MPa (41% of the 214 MPa design ultimate strength). Using the second moment of area of the coupon cross-section, and the applied load, the stress at the strain gauge location was derived. The corresponding strain recorded on the surface of the coupon at this same position (20 mm from the centre of the specimen) was then used to establish the flexural elastic modulus of the sample.

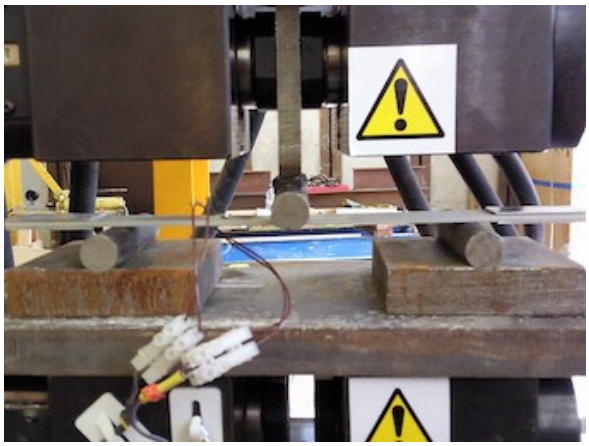

*Figure 19 Flexural testing of coupon*

### 4.3 Results

*Table 7 Retention of coupon flexural stiffness post tensile straining: aged material.*

| Sample | Initial $E_{flex}$ (GPa) | Tensile strain to which sample is subjected (με) | Subsequent $E_{flex}$ (GPa) | % original stiffness retained |
|---|---|---|---|---|
| 1 | 18.4 | 6000 | 19.6 | 106 |
| 2 | 21.5 | 9000 | 10.0 | 46 |
| 3 | 21.3 | 10000 | 5.8 | 27 |

The initial stiffness of the three coupons of aged panel material in Table 7 are seen to be similar. The subsequent stiffnesses vary, depending on the axial tensile strain to which the specimens were subjected before being re-tested in flexure.

It can be seen that a tensile strain of 6,000 με has no detrimental effect on the residual flexural stiffness of the sample, however by imposing 9,000 με the subsequent stiffness is almost halved. Sample 3 was strained to 10,000 με and the subsequent stiffness was shown to be very low. A reduction in stiffness this large would appear at first glance to be attributable to more than resin fracture, as the resin area in cross section is only 30% of the total area. Indeed in the case of Sample 3 some fibre breakage could be heard. This did not occur during straining of Sample 2. Attributing such reductions in stiffness to the resin alone could be explained, and accounted for, by considering fibre distribution in the coupon. It was known that fibre distribution in the cross-section of pultruded GFRP elements is not uniform; the outer ply regions are more resin rich and the central lamina more fibrous. It could therefore be understood how flexural tests might be more sensitive to resin integrity, as the resin is more abundant in the regions more highly strained during flexure.

*Table 8 Retention of coupon flexural stiffness post tensile straining: new material.*

| Sample | Initial $E_{flex}$ (GPa) | Tensile strain to which sample is subjected (microstrain) | Subsequent $E_{flex}$ (GPa) | % of original stiffness retained |
|---|---|---|---|---|
| 1 | 12.5 | 4000 | 13.4 | 107 |
| 2 | 18.7 | 6000 | 20.4 | 109 |
| 3 | 18.7 | 6000 | 19.7 | 105 |
| 4 | 15.0 | 9000 | 14.7 | 98 |
| 5 | 19.4 | 10000 | 19.3 | 100 |

Further tests on new composite material, presented in Table 8, were necessary to demonstrate that the phenomenon of brittle polymer hardening, as characterised by a reduction in strain limit of resin fracture which is age dependent. Flexural tests both before and after an intervening tensile loading yielded very similar results. The fact that the direct axial tensile stress did not affect flexural stiffness indicates that the resin was not affected in coupons of the new material. Coupons of new GFRP do not exhibit a reduction in flexural stiffness when subjected to previous axial tensile strains, up to values of 10,000 με. The conclusion that a reduction in strain limit of resin fracture is age dependent, and to a degree of such great mechanical significance, is an important finding. It confirms that design factors of safety, that should consider this limit, must account for the way in which this limit will change with age.

The initial flexural stiffness of some specimens (S1 of the aged material, and S1-S3 of the new material) was observed to be slightly lower than that found after straining. The stiffness of these specimens could not really increase of course, and the tolerance of the test is revealed to be as much as 10%. Variation between new and old material greater than 10% was deemed to be significant and occurring as a consequence of physical chance in the material with ageing.

With the application of material partial safety factors, the design strength used for design of structural elements in GFRP is typically 60% of the characteristic strength (Bank, 2006). The ultimate tensile strength of the FRP, as defined by Strongwell, is 214 MPa. The useable design strength would therefore be around 0.6×214 = 128 MPa. Using an elastic modulus value of 21.7 MPa (the average tensile modulus from tests

presented in Figure 12), this corresponds to a maximum design strain of 5900 με. This is lower than the strain of 6000 με at which no degradation in stiffness due to polymer hardening was observed and therefore the typical material partial safety factors seem appropriate. It should be noted that in their application as building panels for a site office and visitors centre (not the intended bridge enclosure application) the panel material tested will have experienced an estimated maximum strain no greater than 1000 με in service. This has been verified by a structural design check accounting for both wind and occupancy actions at ultimate limit state on the structural facades.

# 5 Conclusions

A program of mechanical testing of naturally aged composite, taken from the Severn Bridge Visitors' Centre, has assessed the durability of pultruded GFRP. In 17 years, most of the mechanical material properties do not appear to have significantly diminished below design values, despite aesthetic quality suffering due to lack of maintenance.

Coupons of internal material from panels on the south and west-facing façades outperformed those of the weathered external material, in terms of tensile strength, tensile modulus and shear modulus. These elevations are those exposed to the prevailing estuary wind and rain, and those South-facing especially, to a higher degree of UV exposure. Degradation does not appear to have infiltrated the GFRP to a degree that significantly affects 'whole panel' behaviour, and design values therefore appear to be appropriate. East, South and West facing panels, which have experienced direct UV irradiation, all exhibited a slightly reduced stiffness when tested whole with the

weathered external face in tension, as opposed to the internal face in tension.

Coupon testing has demonstrated that the tensile elastic modulus of aged material, on average, meets that of new material. However the tensile strength of the aged material is lower than that of new material. This can partly be accounted for by the observed deficit in fibre content. The comparison afforded between new and old is qualitative, owing to fabrication and material variability remaining unknown factors despite fibre volume fractions being accounted for.

It was apparent that for all old (weathered) panel materials the tensile modulus was lower than the compressive modulus, contrary to most reports in current research. It was hypothesized that 'polymer hardening' had occurred leading to a brittle strain limit for the aged resin. A tensile strain of 9000 με caused severe cracking in the matrix such that subsequent flexural stiffness was reduced by half. A reduction in resin plasticity with age was observed, whilst artificial hydrothermal ageing procedures are known to maintain resin plasticity (Liao et al. 1998; Antoon and Koening 1980) and therefore appear unsuitable in light of these findings.

Resin hardening does not completely explain the relationship between tensile and compressive modulus, because below 6000 με (the region in which the coupon modulus was calculated) the onset of matrix cracking would probably not have been reached. The strong influence of polymer hardening on the stiffness of the composite is very evident, and how this might improve resistance to micro-buckling of fibres in compression is the subject of further research.

## 6 Acknowledgements

A sincere thanks is extended to ARUP and EPSRC, the sponsors of this research, without whom this work would not have been possible. Further deserved thanks is owed the following people: to Masters students Lee Westerman and Dan Culling for assisting with practical laboratory testing, to Mikkel Kragh at Dow Corning for his continuing support throughout this project, to Richard Cooke at Faber Maunsell for providing us with the opportunity to obtain the panels, to James Hennessy of Wring Group for organising the extraction and collection of the panels, and to Richard Irvine at Strongwell for his support in background research of the panels.

## 7 References

- Busel, J.P. (2002). FRP composites industry challenges in developing new markets. Boca Raton: Crc Press-Taylor & Francis Group.
- Boinard, E., Pethrick, R.A., Dalzel-Job, J., and Macfarlane, C.J. (2000). Influence of resin chemistry on water uptake and environmental ageing in glass fibre reinforced composites-polyester and vinyl ester laminates. Journal of Materials Science *35*, 1931-1937.
- Wang, Y.Y., Meng, J.Y., Zhao, Q., and Qi, S.H. (2010). Accelerated Ageing Tests for Evaluations of a Durability Performance of Glass-fiber Reinforcement Polyester Composites. J. Mater. Sci. Technol. *26*, 572-576.
- Compston, P., and Dexter, D. (2008). The effect of ultraviolet (UV) light postcuring on resin hardness and interlaminar shear strength of a glass-fibre/vinylester composite. Journal of Materials Science *43*, 5017-5019.

- Karbhari, V.M., Chin, J.W., Hunston, D., Benmokrane, B., Juska, T., Morgan, R., Lesko, J.J., Sorathia, U., and Reynaud, D. (2003). Durability gap analysis for fiber-reinforced polymer composites in civil infrastructure. J. Compos. Constr. *7*, 238-247.
- Tolf, G., and Clarin, P. (1984). Comparison between flexural and tensile modulus of fiber composites. Fibre Science & Technology *21*, 319-326.
- Strongwell (2010). Composolite fibreglass building panel system. Volume 2010.
- Bank, L.C. (1989). Flexural and shear moduli of full-section fiber reinforced plastic (FRP) pultruded beams. Journal of Testing and Evaluation *17*, 40-45.
- ASTM D 2584 – 02 Standard Test Method for Ignition Loss of Cured Reinforced Resins. Vol. 8.01, American society for testing and materials.
- Ye, B.S., Svenson, A.L. and Bank, L.C. (1995). Mass and volume fraction properties of pultruded glass fibre reinforced composites. Composites, 26(10), pp. 725-731.
- British Standard (2009). Plastics - determination of tensile properties. In Test conditions for unidirectional fibre-reinforced plastic composites. (London: BSi Publications).
- VishayPrecisionGroup (2008). Technical Note 512-1. In Plane-Shear Measurement with Strain Gauges. Toronto: Inter Technology.
- Strongwell (2009). FRP Specifications. Volume 2010.
- Bank, L.C. (2006). Composites for construction : structural design with FRP materials, Hoboken, N.J.: Wiley ; Chichester : John Wiley.
- Liao, K., Schultheisz, C.R. and Hunston, D.L. (1998). Effects of environmental ageing on pultruded GFRP. Composites Part B: engineering, 30(5), pp. 485-493.
- Antoon MK, Koening JL. (1980). The structural and moisture stability of the

matrix phase in glass-reinforced epoxy composites. Journal of Macromolecular Science—Review Macromolecular Chemistry 19(1), pp. 135–173.